Journal of Environmental Chemical Engineering 10 (2022) 108261

Contents lists available at ScienceDirect

Journal of Environmental Chemical Engineering

journal homepage: www.elsevier.com/locate/jece

The promoter effect of Nb species on the catalytic performance of Ir-based catalysts for VOCs total oxidation

Marvin Chávez-Sifontes [a,h], Adrián García [a], Rut Sanchis [a], Clarisse Furgeaud [b,c], Alvaro Mayoral [b,c,d], Raul Arenal [b,c,e], David J. Morgan [f], Stuart H. Taylor [f], Jose Manuel López [g], Tomás García [g,*], Benjamín Solsona [a,*]

[a] Departament d'Enginyeria Química, ETSE, Universitat de València, Av. Universitat, Burjassot, 46100 Valencia, Spain
[b] Instituto de Nanociencia y Materiales de Aragon (INMA), CSIC-Universidad de Zaragoza, 50009 Zaragoza, Spain
[c] Laboratorio de microscopias avanzadas (LMA), U. Zaragoza, C/ Mariano Esquillor s/n, 50018 Zaragoza, Spain
[d] Center for High-Resolution Electron Microscopy (ChEM), School of Physical Science and Technology, ShanghaiTech University, 393 Middle Huaxia Road, Pudong, Shanghai 201210, China
[e] ARAID Foundation, 50018 Zaragoza, Spain
[f] Cardiff Catalysis Institute, School of Chemistry; Cardiff University, Main Building, Park Place, Cardiff CF10 3AT, UK
[g] Instituto de Carboquímica (ICB-CSIC), C/Miguel Luesma 4, 50018 Zaragoza, Spain
[h] Escuela de Química, Facultad de Ciencias Naturales y Matemática, Universidad de El Salvador, Final de Av. Mártires y Héroes del 30 julio, San Salvador, El Salvador

ARTICLE INFO

Editor: V. Victor

Keywords:
Iridium
VOCs
Total oxidation
Alkane
Niobium
Titania

ABSTRACT

Ir/TiO_2 catalysts promoted by niobium have been synthesized, characterized by different complementary techniques, and tested for the total oxidation of a set of alkanes and their mixtures. The addition of appropriate amounts of niobium to Ir/TiO_2 catalysts resulted in a remarkable increase in the catalytic activity compared to the Nb-free Ir/TiO_2 catalysts. The promotion caused by the presence of niobium has been related to the massive presence of isolated IrOx surface species which, interestingly, present remarkable reducibility and, consequently, excellent catalytic activity. Conversely, the IrOx species formed in the catalyst in the absence of niobium also include IrO_2 clusters with lower intrinsic reactivity. Similarly, Nb-loadings exceeding the theoretical monolayer tends to the formation of bulk Nb_2O_5 species on the titania surface that provokes the formation of IrO_2 nanoclusters. A positive influence on the reactivity of non-stoichiometric surface Ti^{3+} species that generates oxygen vacancies is also observed.

1. Introduction

The group of volatile organic compounds (VOCs) with boiling points below 250 °C –at normal pressure– are documented as the most important contributors to global air pollution. Factors such as urbanization and industrialization have been linked to the increment in VOCs emissions. The VOCs emissions are associated with anthropogenic sources, such as petroleum refining, petrochemical processing, solvent use, and many other industrial activities [1–3]. To resolve the VOCs problem there are several strategies based on their mechanisms, recovery technologies, and oxidative approaches. The different chemical characteristics of the compounds and the variety of emission sources are factors that influence the performance of the abatement processes [4,5].

The catalytic oxidation of VOCs is an interesting strategy because the selectivity of the process can be controlled and can be run at relatively lower temperatures than thermal oxidation [6–8]. Some challenges of this process are associated with the excess of oxygen necessary to reach the total oxidation and the expensive costs due to the energy required to heat the gas stream. For that reason, whenever it is possible, catalytic oxidation of VOCs must proceed at low temperatures (room temperature would be ideal) for safety considerations, to reduce operation costs, and for environmental reasons [9].

Noble metal catalysts such as Pt and Pd supported on high-area metal oxides are commonly applied to industrial VOCs total oxidation due to their high intrinsic oxidation activity. Palladium-based catalysts are widely accepted as the best-supported catalysts for oxidation of short-chain alkanes; however, their decreased activity due to the presence of water and multicomponent VOCs, the formation of coke and sensitivity

* Corresponding authors.
E-mail addresses: tomas@icb.csic.es (T. García), Benjamin.solsona@uv.es (B. Solsona).

https://doi.org/10.1016/j.jece.2022.108261
Received 12 April 2022; Received in revised form 5 June 2022; Accepted 10 July 2022
Available online 12 July 2022

to sulphur poisoning are important drawbacks [10]. For this reason, research focused on alternative active phases, such as Iridium, could be highly interesting.

Many reports show γ-Al_2O_3 is the most used support, the relatively low-cost manufacturing process and high specific surface are two main advantages, but that catalyst shows limited stability and consequent deactivation due to severe reaction conditions. Even though γ-Al_2O_3 is the most frequently used support, many studies have demonstrated that the catalytic activities of alumina-supported catalysts are lower than those of catalysts supported on other oxides, such as TiO_2, ZrO_2, and mixed-oxides [11–13].

The research on Ir-based catalysts for VOCs total oxidation can be considered an emergent area. A decade ago, it was reported a comparison study for different noble metal catalysts, this research showed that the preparation method affects the performance of the catalysts. In that study, it was also shown that Ir/TiO_2 presents a reactivity similar to that of Rh/TiO_2, although lower than Pt and Pd-based catalysts [14]. Schick L. et al. have reported the high activity of the Ir/SiO_2 catalyst for oxidation of short-chain alkanes [15]. These Ir catalysts reached higher catalytic activity than catalysts of Pd or Au synthesized in the same way. In that work, an extensive study of catalyst characterization was undertaken and the authors concluded that the calcination temperature can modify important properties of the catalyst, such as the IrO_2 particle's size and the IrO_2 particle's interaction with the support, leading to different reactivity and stability. Reducibility of IrOx species was shown to influence the catalytic activity. Recently, TiO_2 was also reported to be excellent support for iridium applied to the total oxidation of VOCs [16], better than the classical γ-Al_2O_3, which presented a stronger Ir-support SMSI interaction that highly limited its reactivity. Overall, iridium on either silica or titania supports presented similar and high reactivity for the total oxidation of short-chain alkanes; in one case (silica), the reactivity per active site was very high whereas in the other case (titania), the amount of exposed active sites was higher at the same Ir loading.

On the other hand, the addition of a second active component to a noble metal has been shown to enhance the activity of a VOC oxidation catalyst. Those second components are generally added to promote activity and enhance resistance to deactivation. Thus, Taylor M., et al. have referred to niobium on Pd/TiO_2 catalysts [17], although other different promoters, such as vanadium, nickel, cobalt, cerium, and lanthanum have been also studied [18–22]. Most of the studies have been oriented to Pt or Pd/Al_2O_3 catalysts, the promoters (usually with low reactivity themselves) being capable to improve the catalytic activity [18]. The enhanced performance has been explained in terms of different noble metal-support interactions, modifications in the oxidation state, and changes in the dispersion or particle size [19–22].

The use of iridium together with other noble metals has been also reported to present a positive effect on reactivity. Thus, a combination of Ir + Pt supported on ZrO_2 improves the catalytic activity compared to pure Ir/ZrO_2 or Pt/ZrO_2 catalysts, being able to activate hydrocarbons even at low temperatures with high stability in the presence of SO_2 [23]. It seems that there is a synergistic effect between Ir and Pt since iridium sites stabilizes platinum species in suitable oxidation states and this leads to higher reactivity than the pure monometallic catalysts or even higher than a Pd-Pt/ZrO_2 combination.

In another work, Aguilar-Tapia A. et al. reported the combination of Ir and Au supported on TiO_2. This combination showed an improved catalytic activity. Then, Au^0 species tend to avoid the re-oxidation of Ir^0 species, and this was related to the preservation of the activity under reaction conditions [24]. In the same way, Au-Ir/TiO_2 have been reported as good catalysts for toluene total oxidation. For example, in a certain reaction condition, the bimetallic Au-Ir/TiO_2 catalyst reaches ≈ 65% of conversion at 250 °C, while comparable monometallic catalysts (Au/TiO_2 and Ir/TiO_2) reached ≈ 20% and ≈ 5% of conversion, respectively. In addition to the superior activity, the bimetallic catalyst also showed better stability. Thus, in certain conditions, the monometallic catalyst was almost completely deactivated, but the bimetallic catalyst only showed a moderate decrease in activity [25].

The promotional effect of niobium in many catalytic reactions is due to several particular characteristics of this element. For example, depending on the metal oxide, Nb can be introduced in crystalline lattices creating different vacancies that lead to an increase in the catalytic activity [26]. Moreover, its acidity can enhance the adsorption of the hydrocarbon molecule, then favouring in some cases an increase in the reaction rate [27]. In the case of propane combustion, it has been demonstrated that Nb increases drastically the reactivity of Pd/TiO_2 catalysts. This enhanced catalytic activity was ascribed to a modification of the nature of the palladium species and enhanced oxygen mobility [17]. Nb can also affect the redox properties of the active phases favouring reactions that take place by a redox mechanism [28]. As the alkane combustion has been reported to proceed mainly by a redox mechanism in supported Ir catalysts [15], we thought that it was likely that the use of Nb as an additive for iridium catalysts could exert a promotional effect. Conversely, to what happens with Pt or Pd, [29–32], we have not found in the literature one case in which iridium is promoted by a non-noble metal for the total oxidation of VOCs. In the present work, Nb-promoted Ir/TiO_2 catalysts have been tested in the total oxidation of short-chain alkanes, and their performance compared with Nb-free Ir/TiO_2 catalysts. We would like to remark that this is the first case reported in which a promotional effect of doping by an inactive metal (such as Nb) is observed in supported Ir-catalyst for the total alkane oxidation, as it has been often observed in the scientific literature in Pd- or Pt-supported catalysts. Thus, despite the absence of reactivity for niobium species, it will be shown that the addition of niobium to Ir/TiO_2 leads to a remarkable improvement in the catalytic activity of the iridium sites.

2. Experimental section

2.1. Catalysts preparation

The Ir-based catalysts were prepared by incipient wetness impregnation using high purity reagents: Iridium acetylacetonate (chloride-ion free) as the iridium precursor $Ir(AcAc)_3$ (>99.5%, from Sigma-Aldrich), TiO_2 P25 (Degussa) as support and toluene as solvent (>99.8%). A solution containing a suitable mass of the Ir-salt (to give an Ir-content of 1 wt%) was added to the titania support. Then, the catalyst was dried on a hot-plate stirrer at 80 °C for 3 h and calcined for 5 h under static air in an oven at 550 °C (heating rate: 10 °C.min^{-1}). This catalyst was named as 1Ir/Ti.

The Nb-based catalysts were prepared by incipient wetness impregnation adding to the TiO_2 support an aqueous solution of ammonium niobate (V) oxalate $C_4H_4NNbO_9.xH_2O$ (99.9%, supplier). Different concentrations of the Nb-salt were used. The solid mixture was dried on a hot-plate stirrer at 80 °C for two hours and then at 100 °C for 3 h and finally calcined in air at 550ºC for 5 h. At that point, the solid material was ready for iridium incorporation. The iridium was deposited on the solid material following the procedure described above in this section (dried on a hot-plate stirrer at 80 °C for 3 h and calcined for 5 h at 550 °C under air atmosphere). These catalysts were named as 1Ir/xNb/Ti, where x is the theoretical wt% of Nb_2O_5.

For comparison, a Pd/TiO_2 catalyst was prepared in the same way that 1Ir/Ti catalyst but using palladium acetyl-acetonate instead of the iridium salt. This catalyst was named as 1 Pd/Ti.

2.2. Catalyst characterization

The specific surface area of the catalysts was determined from nitrogen adsorption-desorption isotherms at − 196 °C. A Micromeritics ASAP-2020 automated analyser was used. Before the analyses, the catalysts were degassed at 80 °C for 5 h and 10^{-6} Torr. The Brunauer-Emmett-Teller (BET) model was used to calculate the surface areas.

The catalysts were characterized by powder X-ray diffraction (XRD) using a D8 Advanced A25 by Bruker with monochromatic CuKa1 radiation operated at 40 kV and 40 mA. Crystal phases were identified using diffraction data gained from literature via the American Mineralogist Crystal Structure Database.

Catalysts were characterized by Raman spectroscopy. The analyses were undertaken using a Horiba-MTB Xplora spectrometer. The excitation source employed was an Ar ion laser (514.5 nm) operated at 20 mW. The laser was focused on the samples placed on a microscope slide to create a spot size with a diameter of ca. 3 μm.

CO pulse chemisorption analyses were carried out using a Micromeritics Autochem 2920 rig under cryogenic conditions as in [25]. In the standard procedure of this technique, known amounts of CO were pulsed into the sample under a flow of inert gas after degassing the sample at 400 °C. The amount of CO adsorbed in each pulse was quantified by analysing the outlet gas concentration using a thermal conductivity detector (TCD). The pulses were repeated until the sample is fully saturated with the probe molecule. The total amount of CO adsorbed per mass of sample was denoted as V_{ads} ($cm^3 \cdot g^{-1}$). The metallic surface area (SA_{metal}) was then calculated as shown in Eq. (1):

$$SA_{metal}=(V_{ads}/22{,}414)\cdot SF\cdot N_A\cdot A_{metal} \quad (1)$$

where SF is the stoichiometric factor of the number of adsorbed probe molecules per metallic surface atom (two CO molecules per surface iridium site were assumed), A_{metal} is the cross-sectional area of the metal (0,0769 nm^2 for Ir) and N_A is Avogadro's number.

Ammonia temperature programmed desorption (NH_3-TPD) experiments were conducted on a Quantachrome ChemBET Chemisorption analyser equipped with a TCD. The catalysts (250 mg) were first heated to 400 °C (15 °C·min^{-1}) under He (30 mL·min^{-1}) and held at temperature for 2 h. After cooling to 150 °C, the catalysts were exposed to NH_3 for 0.5 h at a flow rate of 30 mL·min^{-1}, after which, the samples were heated to 500 °C (10 °C·min^{-1}) under He (30 mL·min^{-1}).

Oxygen temperature programmed desorption (O_2-TPD) experiments were conducted on a Quantachrome ChemBET Chemisorption analyser equipped with a TCD. The catalysts (250 mg) were first heated to 120 °C (15 °C·min^{-1}) under He (30 mL·min^{-1}) and held at temperature for 2 h. After cooling to 30 °C, the catalysts were exposed to O_2 atmosphere (5% O_2 / 95% He) for 1 h at a flow rate of 30 mL·min^{-1}, after which, the samples were heated to 600 °C (10 °C·min^{-1}) under He (30 mL·min^{-1}).

Temperature programmed reduction (TPR) analyses have been performed in a Micromeritics Autochem 2920 instrument equipped with a thermal conductivity detector. The reduction step has been carried out in a 50 mL·min^{-1} flow of 10% H_2/Ar between 40 °C and 400 °C with a heating rate of 20 °C·min^{-1}.

Electron microscopy observations were carried out in two different spherical aberration corrected FEI microscopes Titan High-base and Titan Low base (correcting the objective and condenser system respectively), both operated at 300 kV. Chemical analyses were carried out in the probe corrected microscope that incorporates an Oxford silicon drift detector for X-ray energy-dispersive spectroscopy (EDS) and a Tridiem Gatan Energy Filter for electron energy loss spectroscopy (EELS). Prior to observation, the samples were dispersed onto carbon-coated copper microgrids.

X-ray photoelectron spectroscopy (XPS) measurements were performed using a Thermo K-Alpha$^+$ photoelectron spectrometer. Powdered samples were pressed into wells of a copper plate used for the analysis of loose powders. A micro-focused Al-kα X-ray source operating at 72 W (6ma x 12 kV) was used operating in the "400-micron spot" mode of operation. Data were acquired at a pass energy of 40 eV for high-resolution scans and 150 eV for survey scans at step sizes of 0.1 and 1.0 eV respectively. Charge compensation of the insulating samples was achieved using a combination of low energy electrons and argon ions resulting in a C(1 s) energy for adventitious carbon of 284.8 eV, all binding energies are assumed to have an associated error of ± 0.2 eV. Data were analysed using CasaXPS v2.3.24 PR1.0 [33] using Scofield sensitivity factors and an electron escape depth dependence according to the TPP-2 M equation [34].

2.3. Catalytic tests

The catalytic performance of the prepared materials was studied using 100 mg of the catalyst for the total oxidation of alkanes (mainly propane). The catalyst was sieved to obtain a particle size between 0.3 and 0.75 mm and loaded into a quartz tube micro-reactor (øID=12 mm). The gaseous feed composition was 0.8/20/79.2 mol.%, for the alkane (propane, ethane, or methane), oxygen, and helium, respectively. The flow rate employed was fixed at 50 mL.min^{-1}. In some selected experiments, methane, ethane, and propane were simultaneously fed. In this case, the gaseous feed composition was 0.8/0.8/0.8/19.6/78.0 mol%, for propane, ethane, methane, oxygen, and helium, respectively. The effect of the presence of water steam (8 mol%) and/or CO_2 (2 mol%) was also studied. In these experiments the feed consisted of propane/CO_2/water/O_2/He = 0.8/0–2/0–8/17.8–19.6/71.4–78.0 mol%.

The reactor was heated by a ceramic system, which covers the quartz tube micro-reactor. The heating system is equipped with a thermocouple connected to a temperature controller. The catalytic tests were undertaken between 150 and 500 °C. The temperature was increased by 25 °C steps. Before the analyses, the system was held for 30 min at fixed temperatures. For each temperature, two analyses were registered, and the result corresponds to the average of both. In all the cases, the results obtained at the same temperature were indistinguishable.

The outlet gas was analysed by injections into a Hewlett-Packard gas chromatograph equipped with a Carbosieve-S and a Porapak Q column. Once the reaction was completed, the oven was switched off and the catalyst was allowed to slowly cool down under a stream of pure helium.

3. Results and discussion

Total oxidation of short-chain alkanes was studied, especially that of propane, using Nb- promoted Ir/TiO_2 catalysts. Representative physicochemical characteristics of these catalysts are shown in Table 1.

The activity of both the TiO_2 support and the Ir-free Nb/TiO_2 catalysts was very low compared to the Ir-containing catalysts. A significant difference in the activation temperature for propane was observed, with temperatures of 425 °C for the bare support or Nb/TiO_2 catalyst, whilst for the iridium containing catalysts the temperature was 225 °C. Therefore, it can be concluded that iridium sites are likely to be those responsible for the observed activity at low temperatures.

For all Ir-containing samples, the only reaction product containing carbon was CO_2 with C-balances always being close to 100 ± 3%. In the case of the Ir-free catalysts, some propylene and CO were also observed

Table 1
Characteristics of the Ir/Nb/TiO_2 catalysts.

Catalyst	Ir		Nb_2O_5[a]	Nb surface	Surface	Dispersion
	Nominal (wt%)	ICP (wt %)	(wt%)	Coverage[b] (%)	Area (m^2/g)	of Ir[c] (%)
TiO_2	–	–	–	–	55	–
1Ir/ Ti	1	1.1	–	–	51	26.7
5 Nb/Ti	–	–	5.0	74	51	–
1Ir/1 Nb/ Ti	1	1.1	1.0	14	50	41.2
1Ir/2 Nb/ Ti	1	1.0	2.0	29	52	37.3
1Ir/5 Nb/ Ti	1	1.1	5.0	74	50	51.8
1Ir/10 Nb/ Ti	1	1.0	10.0	158	50	37.6

[a] Nominal value, [b] Total monolayer coverage: 5.8 Nb atoms/nm^2 [33,34], [c] by CO chemisorption CO/Ir= 2

although in both cases with low selectivity.

Fig. 1 A shows the evolution of a typical light-off curve representing the alkane conversion with the reaction temperature in the total oxidation of propane for the different catalysts. Nb-free Ir/Ti catalyst is in all cases less reactive than any of the Ir/Nb/Ti catalysts. As the Nb/Ti catalyst presents low reactivity, the enhanced performance of bimetallic catalysts is not the result of the addition of both iridium and niobium active sites, but the modification of the active iridium sites, see Table 2. Moreover, the amount of Nb is very important since there is a maximum for the Nb-loading of 5 wt%. Then, the catalytic activity follows the trend Nb/Ti < << Ir/Ti < 1Ir/10 Nb/Ti < 1Ir/1 Nb/Ti, < 1Ir/2 Nb/Ti < 1Ir/5 Nb/Ti. Interestingly, the addition of the optimal amount of Nb shifts the light-off curve ca. 50ºC towards lower temperatures compared to the Nb-free Ir/Ti catalyst. For a comparative purpose, a typical catalyst (Pd supported on TiO_2) for total oxidation of VOCs was synthesized and tested for the reaction. This Pd/Ti catalyst was prepared in the same way and with the same noble metal loading (1 wt%) that the Ir/Ti sample. Pd/TiO_2 catalyst shows a higher reactivity than Ir/TiO_2 counterpart but, importantly, lower than the optimal Nb-promoted Ir/Ti catalyst (the catalytic activity per gram of catalyst was higher by a factor of ca. 2).

Fig. 1B shows the comparison of the light-off curves for propane, ethane, and methane oxidation using the optimal 1Ir/5 Nb/Ti catalyst. As expected, the higher the chain of the alkane the higher the reactivity observed.

The stability of 1Ir/5 Nb/Ti catalyst was tested using different substrates, maintaining the optimal reaction conditions for propane conversion as probe molecule (Fig. 2A). All the tests were firstly undertaken at a reaction temperature of 350ºC. A 25-hour experiment was conducted feeding propane and the same conversion was observed for the whole experiment. Similar, but shorter (ca. 8 h), experiments were undertaken with methane and ethane also showing excellent stability but reduced conversion due to the low reaction temperature used for shorter alkanes. Fig. 2 B shows the evolution with the time on line at higher reaction temperatures for ethane and methane conversion (400 and 450 ºC respectively). These higher reaction temperatures were chosen in order to see the stability of the catalyst at higher alkane conversions. For both conditions a highly stable behaviour was observed.

Another test was undertaken using the three alkanes together to see the influence of co-feeding (Fig. 2A). Feeding the mixture, the conversion of all the substrates decreased if compared to the experiments in which the alkanes were tested alone. The fall in conversion observed was different for each alkane in a way that the shorter hydrocarbon chain, the higher decrease in activity was evidenced. Then, in the case of propane, the conversion decreased ca. 7% points (down from 72%), for ethane ca. 13% points (down from 38%), and methane ca. 4% points (down from 9%). Competitiveness of the active sites for adsorbing/reacting the reactant molecules can be related to this behaviour. On the other hand, the different extent of the drop of reactivity is likely related to the higher adsorption capacity of the longer alkanes. Interestingly, in this experiment, no variation of the conversion was observed along the reaction time for any of the alkanes employed.

Table 2
Total oxidation of propane on Nb-doped Ir/TiO_2 catalysts at 275ºC[a].

Catalyst	Catalytic activity[b]	T50[c] (ºC)	Activity per Ir active site[d]	TOF[e] (s^{-1})
1Ir/Ti	7.30	375	8.85	33.2
1Ir/1 Nb/Ti	25.02	352	30.3	81.3
1Ir/2 Nb/Ti	29.20	345	35.4	95.0
1Ir/5 Nb/Ti	57.98	320	70.3	132
1Ir/10 Nb/Ti	23.63	355	28.7	76.2
5 Nb/Ti	0	> > 425	–	–

[a] Data at conversions lower than 15%. Reaction conditions in text, 0.8 vol% of C_3 in synthetic air, 0.1 g, 50 mL·min^{-1}.
[b] grams of propane reacted per kg cat per h
[c] T50 is the reaction temperature required to achieve 50% conversion
[d] 10^{-4} Molecules of propane reacted per Ir atom per s
[e] 10^{-4} Molecules of propane reacted per exposed Ir atom per s

At this point, we have seen that one of the Nb-promoted Ir/Ti catalysts shows stable behaviour with high reactivity, which is higher not only than Ir/Ti catalyst with the same noble metal loading but also higher than Pd/Ti catalyst. Then, Nb-free and Nb-promoted Ir/Ti catalysts have been characterized to find an explanation for the positive effect of niobium.

Some characteristics of Ir and/or Nb supported on titania catalysts are presented in Table 1. The titania support presents a specific surface area of 55 m^2g^{-1}, a value somewhat higher than that of the catalysts with iridium or niobium incorporated (between 45 and 50 m^2g^{-1}). Over the titania, several Nb loadings have been added (1, 2, 5, and 10 wt% Nb) which, as the total monolayer surface coverage takes place with 5.8 Nb atoms/nm^2 [35,36], corresponds to theoretical coverages from 10% (1 wt%) to 158% (10 wt%) of the monolayer.

To estimate the amount of active Ir sites, the catalysts were submitted to CO chemisorption. An adsorption stoichiometry of CO/Ir = 2 was assumed, although this point can be controversial [37,38]. In fact, the CO/Ir ratio can be different depending on the level of aggregation of the iridium species since low aggregated Ir species could adsorb more CO molecules than larger iridium clusters. However, this CO/Ir ratio can be considered a suitable approach for a comparative study. According to this, for all Nb-promoted Ir/TiO_2 catalysts the iridium dispersion is higher than that in the Nb-free Ir/TiO_2 catalyst (dispersion of ca. 26%). The amount of niobium in the catalyst exerts a subtle effect as the

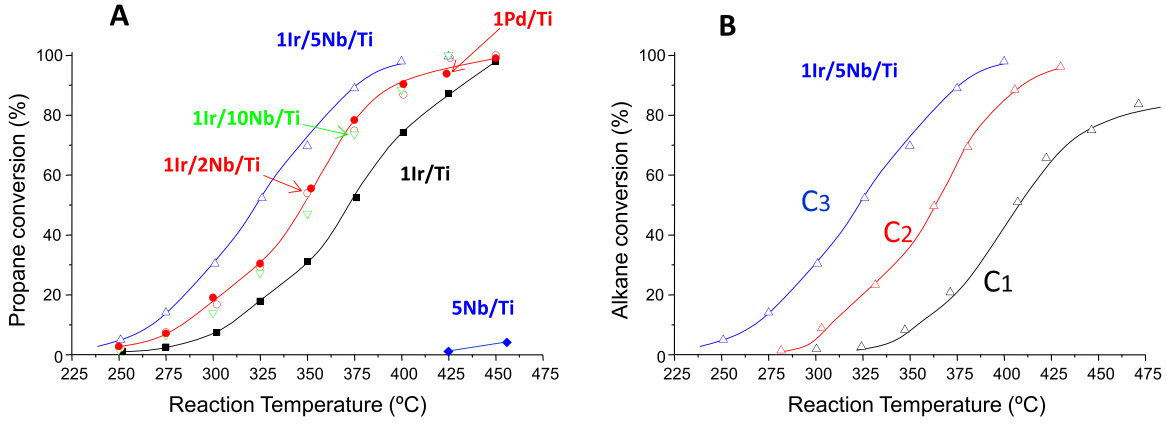

Fig. 1. (A) Variation of the propane conversion with the reaction temperature for Nb/ and/or Ir/TiO_2 catalysts. (B) Variation of the C_1 to C_3 conversion with the reaction temperature for 1Ir/5 Nb/Ti catalyst. Reaction condition in text.

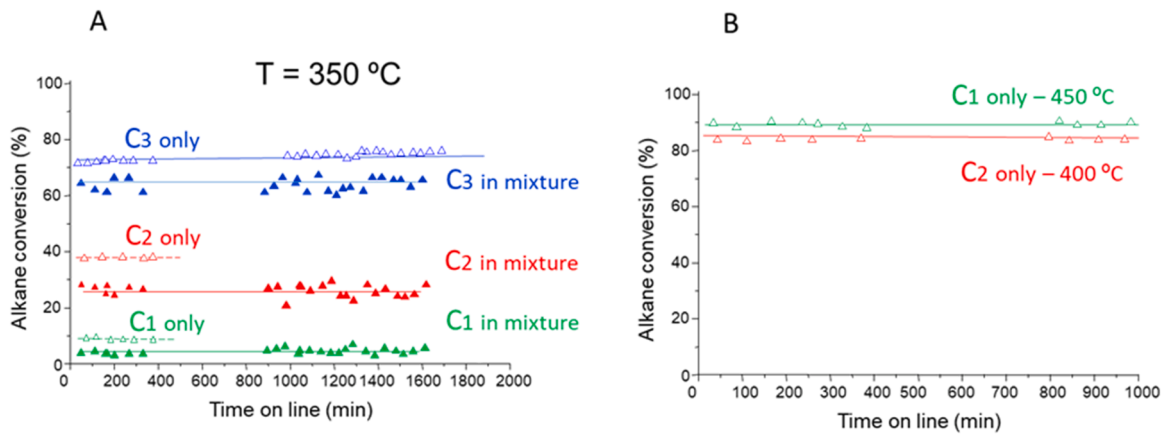

Fig. 2. Catalytic stability for 1Ir/5 Nb/Ti catalyst. (A) Evolution of the alkane conversion with the reaction time for both independent experiments or in a C_1-C_2-C_3 mixture. Reaction condition in text and reaction temperature of 350ºC, (B) Evolution of the ethane conversion (at 400 ºC) and methane conversion (at 450ºC) with the time on line. Remaining reaction condition in text.

Ir/Nb-catalyst with 5 wt% Nb presents the highest Ir dispersion (ca. 52%) compared to other Nb-loadings (ca. 39%). The Ir dispersion values obtained for the 1Ir/1 Nb/Ti, 1Ir/2 Nb/Ti and 1Ir/10 Nb/Ti samples (41.2%, 37.3% and 37.6% respectively) can be considered broadly similar due to the experimental error of around 5% associated to the CO chemisorption measurements. For the catalyst without iridium (5 Nb/Ti) the CO uptake was null so it can be concluded that CO is chemisorbed on the iridium sites.

XRD patterns of the catalysts employed are shown in the supplementary information (see Fig. S1a). In all cases, the diffractograms are very similar to that of the TiO_2 support, which consists of a mixture of anatase (JCPDS: 21–1272) as a majority phase and rutile (JCPDS:21–1276). Only in the 1Ir/10 Nb/Ti catalyst low-intensity reflections of orthorhombic Nb_2O_5 (JCPDS: 30–0873) have been observed (see Fig. S1b). The absence of any Ir-containing crystalline phase reflection is not surprising, as higher loadings could be needed. Additionally, this fact could be indicative of either the amorphous character of the Ir species, and/or the presence of well-dispersed IrO_2 clusters/nanoparticles on the external surface.

Raman spectra recorded from 200 to 1200 cm^{-1} of selected catalysts are shown in Fig. 3. The main bands can be ascribed to anatase (640, 510, 390 cm^{-1}) and rutile (shoulders at 450 and 605 cm^{-1}). These results are in line with XRD data. Interestingly, a shift towards lower frequencies has been observed for the catalysts that contain Ir (both with or without Nb), whereas no shift is observed when only Nb was added. No apparent differences can be observed between the spectra of pure titania support and that of Nb/Ti catalyst. This observation suggests that the Ti-O bonds become weaker when iridium is added. Then, a displacement of the density of charge from titania to iridium species takes place.

The presence of bulk Nb_2O_5 (neither hexagonal nor monoclinic) or Nb-species with lower aggregation cannot be clearly observed by Raman. This is likely due to the high dispersion of the Nb-species or even to the masking by the high intensity of the anatase and rutile bands. We could not observe Raman bands corresponding to either terminal Nb=O bonds at 970–1030 cm^{-1} typical of isolated Nb species or bands assigned to bridging Nb–O–Nb bonds associated with non-bulky surface polymerized Nb-species which appear at 850–980 cm^{-1} [39,40].

In order to have a better understanding of the catalysts, detailed TEM studies were undertaken on selected samples. Low-magnification TEM images (Fig. 4a and 4b) show the morphology of the TiO_2 materials, corresponding to the Nb-free Ir/TiO_2 catalyst. The electron diffraction analysis (selected area electron diffraction (SAED)) has been performed on these NPs (see supporting information). The electron diffraction patterns (EDP) of Fig. S2a were indexed assuming anatase structure type, while the analysis of individual TiO_2, Fig. S2b, corroborates the

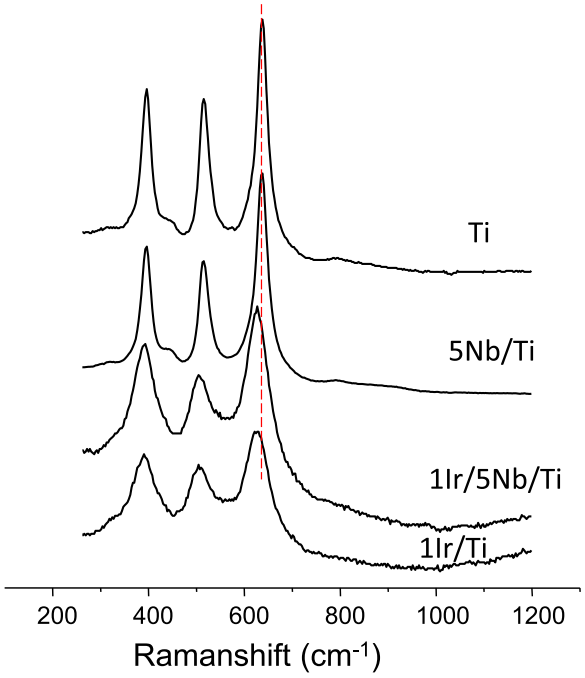

Fig. 3. Raman spectra of selected Ir/Nb_2O_5/TiO_2 catalysts.

single-crystal nature of each particle. As shown in Fig. S2c, particles between 10 and 30 nm were mainly observed.

Detailed observation was performed utilizing spherical aberration (C_s-corrected) scanning transmission electron microscopy (STEM), coupled with a high angle annular dark field detector (HAADF) sensitive to the atomic number of the elements [41], see Fig. 4. In here, besides the clear observation of different TiO_2 crystals it is possible to appreciate different species of iridium incorporated in this material adopting three different configurations:

- In one of these configurations, Ir-containing clusters/nanoparticles are supported on the TiO_2 NPs. These Ir nanoparticles with a mean diameter of 1.4 nm (Fig. S2d) can be assigned to an IrO_2 *fcc* structure (*Fm*-3*m* space group), as elucidated from the FFT diffractogram shown in the inset of Fig. 4f.
- The second observed configuration is the one of Fig. 4(c, e). In this case, Ir is incorporated in the TiO_2 anatase structure. This

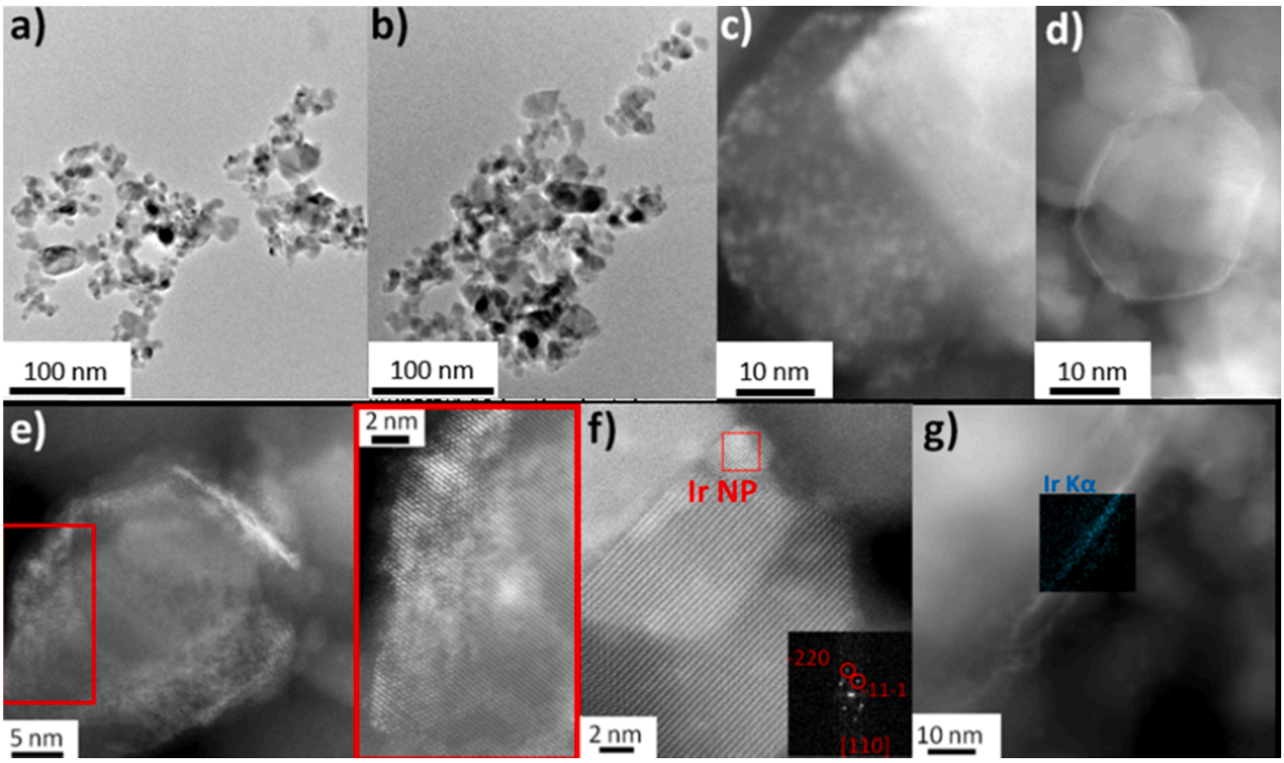

Fig. 4. TEM study of 1Ir/Ti catalyst. (a) and (b) show the low-magnification TEM images of TiO_2 nanoparticles with 1% Ir content. (c) and (d) show C_s-corrected STEM-HAADF images of TiO_2 nanoparticles with 1% Ir content. (e), (f) and (g) show the STEM images of TiO_2 nanoparticles with 1% Ir content. (f) FFT diffractogram of the highlighted Ir nanoparticle is inserted. (g) EDS map of Ir Kα radiation is inserted in this HAADF-STEM image.

configuration can be clearly appreciated in the magnified area shown in Fig. 4e, corresponding to the red rectangle.

- And finally, we have also observed Ir segregation at TiO_2 nanoparticles surface creating an oxidized Ir shell around TiO_2 NPs (Fig. 4g).

Further investigations were carried out on the optimal Nb-promoted Ir/Ti catalyst (1Ir/5 Nb/Ti) to elucidate any significant differences upon the incorporation of Nb into the system (Fig. 5). Low-magnification image of the 1Ir/5 Nb/TiO_2 material is depicted in Fig. 5a, where faceted TiO_2 nanoparticles can be clearly identified. Interestingly, some of them display a strong signal on the surface, which due to the stronger scattering factor of Ir atoms, can be attributed to the presence of this metal coating the TiO_2 crystallites. A closer observation of a very-well crystallized TiO_2 NP of dimensions of 60 × 40 nm with truncated rectangular shape is presented in Fig. 5b. A very fine layer of what corresponds to Ir atoms can be observed on the surface of this particle. A closer observation of the edge of this particle is shown in Fig. 5c, revealing the lattice fringes of the TiO_2 and the brighter and stronger signal that corresponds to an atomic layer (one atom thickness) associated with the incorporation of Ir, and an ordered fashion into the TiO_2 network (a magnified thermal coloured view of this layer is shown inset).

Additional analysis was carried out on another crystal, see Fig. 5(d-f). For this case, additional contrast to that observed on the surface can be visualized in the central part of this TiO_2 particle. The two areas of analysis have been marked by red (central) and yellow (surface) dashed rectangles. The magnified observation of these areas is also presented revealing a perfect bright spot distribution. Such a large contrast variation is due to the presence of Ir atoms, which, based on the clear periodicity, were incorporated into the TiO_2 framework. The square-shaped arrangement corresponds to the [001] of rutile (*P*42/*mnm*) and proves how the Ir has been incorporated into the TiO_2 structure (of both rutile and anatase TiO_2 phases). A magnified observation of the edge of this particle also reveals the atomic incorporation of the Ir into the TiO_2 structure in agreement with it occurred in the central part.

To further corroborate these statements, chemical analyses were carried out by means of EDS spectroscopy; Fig. 5e corresponds to the chemical maps obtained from the particle shown in Fig. 5d observing the homogeneous distribution of the Ti and O elements corresponding to the TiO_2. Although Ir is dispersed along the entire support, the signal is stronger on the surface of the crystallite in agreement with the observation of the edge, dashed yellow rectangle. Nb signal was significantly lower in comparison with the Ir but EDS also evidenced the homogenous Nb distribution over the TiO_2 particle. The chemical spectrum profile, Fig. 5f, clearly corroborates the chemical composition expected: Ti and O of the support and Ir and Nb corresponding to the metals incorporated. The additional signals observed are Cu and C coming from the TEM grid used and Si, which is an impurity.

Fig. 6 shows the STEM information on the Ir sample with the highest Nb loading (1Ir/10 Nb/Ti). In this catalyst, both metals, niobium, and iridium can be seen on the surface of the titania. Conversely to the 1Ir/5 Nb/Ti catalyst, some Nb_2O_5 particles can be seen on the surface of the titania crystals, in agreement with that observed by XRD. Iridium is in the form of isolated atoms that, on the surface, agglomerate forming IrO_2 clusters. In some cases, an almost continuous layer of 1 nm coating the titania crystals is observed. Despite the disordered nature of the metal oxide clusters, in a few cases, they present a crystalline nature. Overall, Ir and Nb are mainly intermixed and in some cases, nanoclusters of iridium oxide are located over the Nb_2O_5 particles but we have not found evidences of the formation of Ir/Nb alloy Nevertheless, we cannot completely rule out this possibility due to the good dispersion of Nb species over TiO_2.

Electron microscopy analysis was carried out on the 1Ir/5 Nb/Ti catalyst after reaction test in order to check the thermal stability of the surface species. No significant differences have been observed in the material after reaction, where only (in certain regions) Nb species would agglomerate forming small nanoparticles in the range of 2 nm; however,

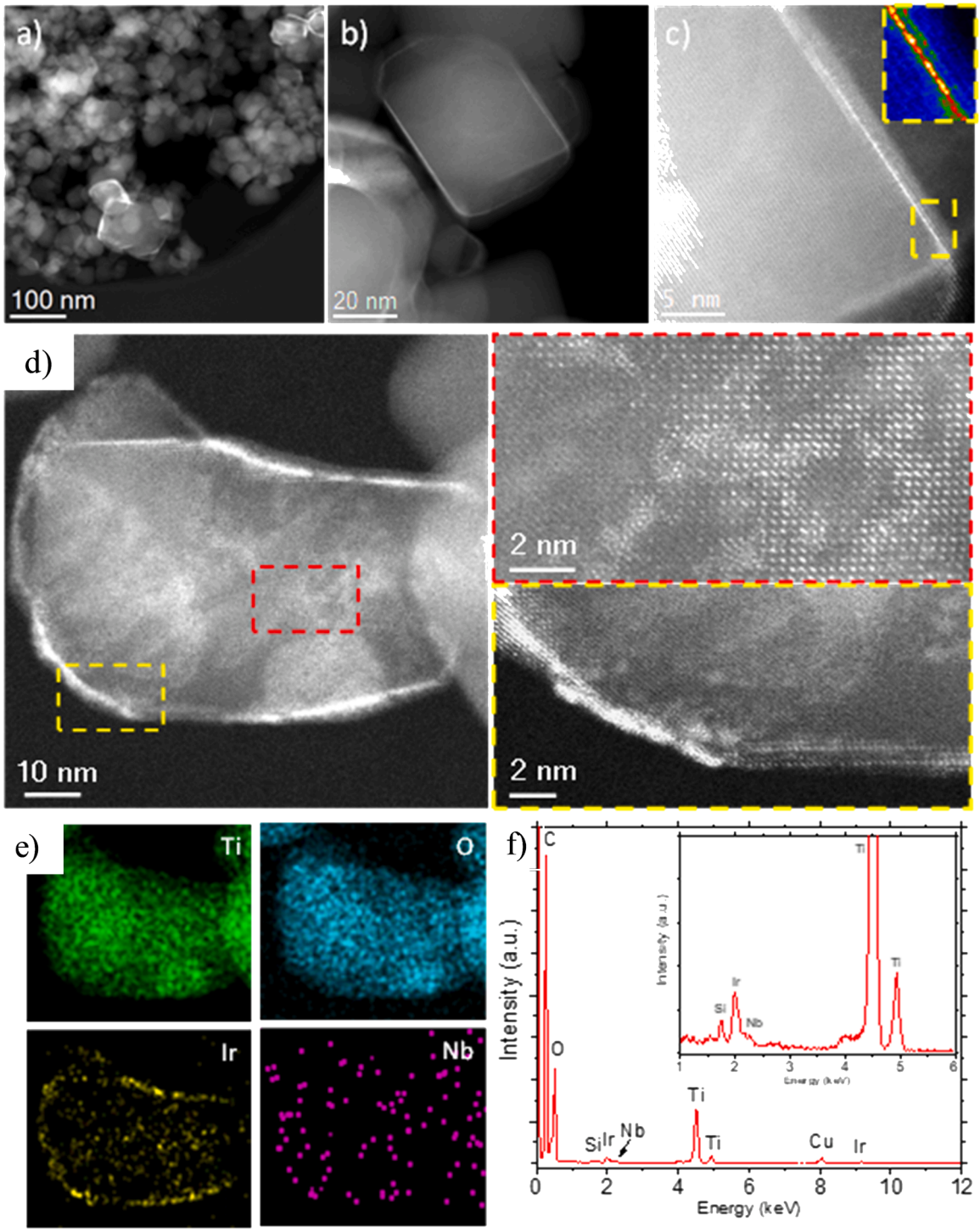

Fig. 5. C_s-corrected STEM-HAADF analysis of 1Ir/5 Nb/Ti sample. (a) Low-magnification observation. (b) Closer observation of a few TiO_2 NPs. c) Atomic-resolution data of the corner of the particle shown in b. (d) C_s-corrected STEM-HAADF image of a TiO_2 nanoparticle of 1Ir/5 Nb/Ti catalyst. The areas that were zoomed in are marked by dashed rectangles. The correspondent magnified images are also presented and framed by red and yellow rectangles for the centre and the edge, respectively. (e) Chemical maps were obtained from the image shown in (d). (f) EDS spectrum proving the existence of Ti, O, Nb, and Ir. C and Cu are owed to the TEM grid used, while the Si is an impurity.

IrOx remained very similar as in its original form (see Fig. S3 a, b and c). Chemical maps were also performed observing the same chemical distribution as for the as-synthesized sample (Fig. S3d). Additionally, the used sample was also submitted to XRD analysis (Fig. S1c). XRD spectrum did not exhibit peaks corresponding to reflections neither from Nb nor from Ir, which confirms that these species are highly dispersed even after reaction test."

TPD-NH_3 study indicates important differences regarding the acidity of the catalysts (Fig. 7). 1Ir/Ti catalyst presents acid sites both weak and strong. The presence of niobium leads to a slight decrease in the number of acid sites compared to the base Ir/Ti catalyst. However, the most important differences lie on the strength of those acid sites. Then, the presence of niobium tends to decrease the number of strong acid sites (those appearing from 250 to 300ºC). This decrease is most notorious in

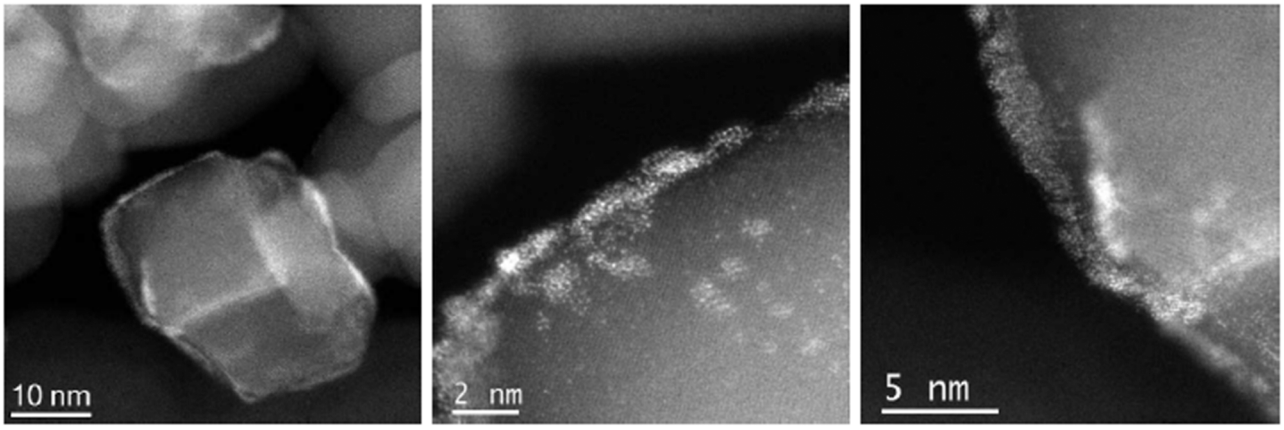

Fig. 6. Representative TEM images of the Ir sample with the highest Nb loading (1Ir/10 Nb/Ti).

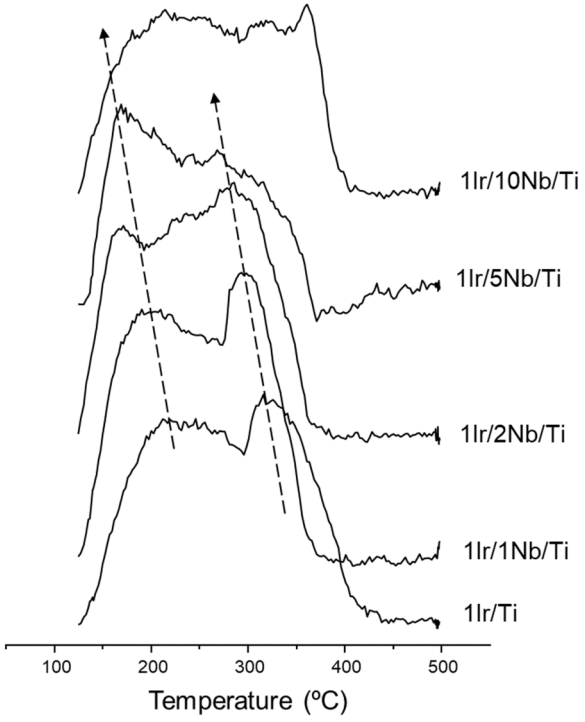

Fig. 7. Temperature programmed desorption of ammonia on Ir/Nb/Ti catalysts.

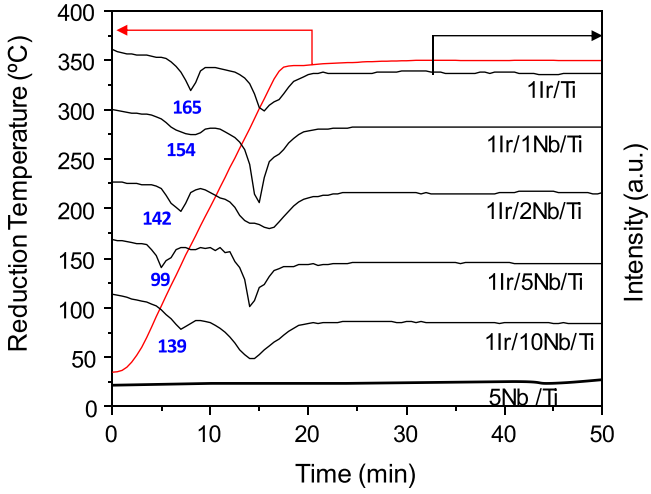

Fig. 8. Temperature programmed reduction of Ir/Nb/Ti catalysts.

the catalyst with 5 wt%Nb. Besides, these strong acid sites become weaker when adding niobium since a shift towards lower temperatures of this desorption band is clearly observed. However, when higher Nb-loadings are added (10 wt%Nb) desorption at higher temperatures corresponding to strong acid sites are observed, which is probably due to the formation of Nb_2O_5 clusters. Interestingly, the addition of Nb to the Ir/Ti sample also weakens the weak acid sites (those appearing below 200–250ºC) since a shift towards lower temperatures is clearly observed for those catalysts with 2 and 5 wt%Nb.

As the total oxidation of alkanes on iridium catalysts have been reported to proceed through, at least partly, a redox mechanism, temperature-programmed reduction experiments have been undertaken on the Ir/Nb/Ti catalysts (Fig. 8). As no apparent band has been observed in the Ir-free sample in the temperature range studied (until 400ºC), we can conclude that these bands are the result of the reduction of the IrOx species. In usual reduction experiments, for the NbOx-species reduction, temperatures of 700ºC and higher are required. Two main reduction bands have been observed for all the Ir-containing samples. The maximum of the first band is at ca. 150ºC and the second one at ca. 330ºC, which corresponds to IrOx species interacting with different strengths with the support. It can be observed that the reductions of the sample without niobium take place at slightly higher temperatures than those of the Ir-catalysts with niobium, especially in the samples with the highest loadings. It is noteworthy the highest reducibility was observed for the 1Ir/5 Nb/Ti catalyst with the first peak appearing at temperatures below 100ºC. Then, it seems that the addition of niobium favours the reducibility of the IrOx species although an excess of Nb is not positive, possibly due to the formation of IrOx species over Nb_2O_5 clusters which presents lower reducibility.

Results from the XPS analysis of the catalysts are presented in Table 3 and Fig. 9. For niobium doped catalysts, the Nb is present predominantly in the 5 + oxidation state (binding energy, 207.4 eV, red peaks in Fig. 9b) with small concentrations of Nb^{4+} (206.2 eV, purple peaks in Fig. 9b). Analysis of the Ir oxidation state and content of the respective catalysts was made on the Ir(4 f) peaks; however, there is considerable overlap with the Ti(3 s) peak and also some interference from the Nb (4 s) state (see Fig. 9a, where blue = Ir, green = Ti and red = Nb). Even if difference spectra were used to generate the Ir signal and compared between all catalysts, the same peak shape was found in all cases. For these catalysts, Ir is found in the 4 + oxidation state and likely present as IrO_x, as evidenced by the asymmetric peak shape (see Fig. 9d). However, the observed binding energy of 61.4 eV is somewhat lower than that of bulk IrO_2 (ca. 62 eV, [42]), but this lower binding energy may be due to

Table 3
XPS derived atomic concentrations (at%) for Ir, Nb, and Ir/Nb TiO_2 catalysts.

Catalyst	Concentration / at%					Ratio	Ratio
	C	Ti	O	Nb	Ir	Ti^{4+}/ Ti^{3+}	Nb^{4+}/ Nb^{5+}
1Ir/TiO_2	23.92	22.71	53.16	n/a	0.21	35.0	n/a
1Ir/0.5 Nb/ TiO_2	19.63	23.54	56.14	0.30	0.40	37.6	0.11
1Ir/1 Nb/ TiO_2	20.79	23.34	54.97	0.53	0.40	44.8	0.06
1Ir/2 Nb/ TiO_2	23.47	22.23	53.16	0.73	0.40	40.9	0.06
1Ir/5 Nb/ TiO_2	19.02	21.63	56.74	2.12	0.50	31.8	0.12
1Ir/10 Nb/ TiO_2	19.71	21.10	56.05	2.57	0.56	32.5	0.09
5 Nb/TiO_2	17.26	22.35	58.02	2.36	n/a	73.5	0.04

incorporation into the TiO_2 lattice and charge transfer to the Ir atoms. Incorporation of the metals into the TiO_2 lattice is evidenced by the evolution of Ti^{3+} sites (see Fig. 9e), supporting the Raman and (S)TEM results. The O1s spectra for all catalysts are virtually identical (see Fig. S4), with a Ti-O lattice oxide peak centered at 530 eV and a peak assigned as hydroxide at ca. 531.5 eV. For bare P25, the O(lattice)/Ti ratio is found to have the expected value of 2.0, whereas for all other samples, the value is slightly higher at 2.2, indicating an excess of oxygen which is attributed to the Ir and Nb oxides.

In order to explore further the role of surface and subsurface oxygen on governing catalyst activity, a series of oxygen TPD experiments were performed (Fig. 10). The oxygen peak ca. 200 °C can be expressed as the active physical/chemical oxygen species adsorbed on the surface (Os) of the catalyst and that desorbed at ca. 350 ºC as the subsurface lattice oxygen (Oss) [43]. Although the results for all catalysts were broadly similar, some differences mainly in the desorption subsurface oxygen zone, both in terms of desorption temperature and magnitude can be observed. It seems that the incorporation of increasing amounts of Nb decreases the quantity of desorbed Oss as the area of the peak ca. 350 ºC is reduced. Interestingly, the desorption temperature of Oss shifts to lower values, pointing out that O species are more reactive when adding Nb to the Ir catalyst. The catalyst with 5 wt% seems to be the optimum, since a balance between the number of Oss and their mobility is reached.

4. Discussion

The addition of Nb to the Ir/TiO_2 catalyst has meant an increase in the catalytic activity by a factor of 8 in spite of the fact that Nb/TiO_2 is inactive in the range of temperatures studied. This enhancement can be related to several factors. On one hand, the amount of available iridium active sites determined by CO chemisorption is higher in the bimetallic Ir/Nb/TiO_2 catalysts than in Nb-free Ir/TiO_2 catalysts. However, the increased activity is remarkably higher than that expected by the higher amount of iridium active sites. In fact, the turnover frequency, which only considers the exposed iridium sites, increases ca. 500% for the optimal Ir/Nb/Ti catalyst compared to the Nb-free Ir/TiO_2 catalyst.

This reaction takes place on iridium sites through a redox Mars-Van Krevelen mechanism. In this mechanism, the VOC molecule is transported from the gas phase towards the catalyst, where it absorbs and reacts with an oxygen atom originating from the iridium oxide active site. Hence, an oxygen vacancy is generated during this reaction in the iridium oxide (reduction) and therefore, an improvement in the reducibility could highly affect the catalytic performance. Afterwards, the iridium oxide fills this vacancy with surface oxygen originating from the gas phase (oxidation). This re-oxidation step of the redox cycle is apparently less important than reducibility as the iridium easily oxidizes into IrO_2. Accordingly, it has been observed improved reducibility of the IrOx sites in the Nb-containing samples, this improvement being noteworthy in the catalyst with 5% Nb (1Ir/5 Nb/Ti catalyst). Fig. 11 plots the TOF vs the temperature of the maximum of the first reduction peak. As can be observed in that figure, the turnover frequency increases when

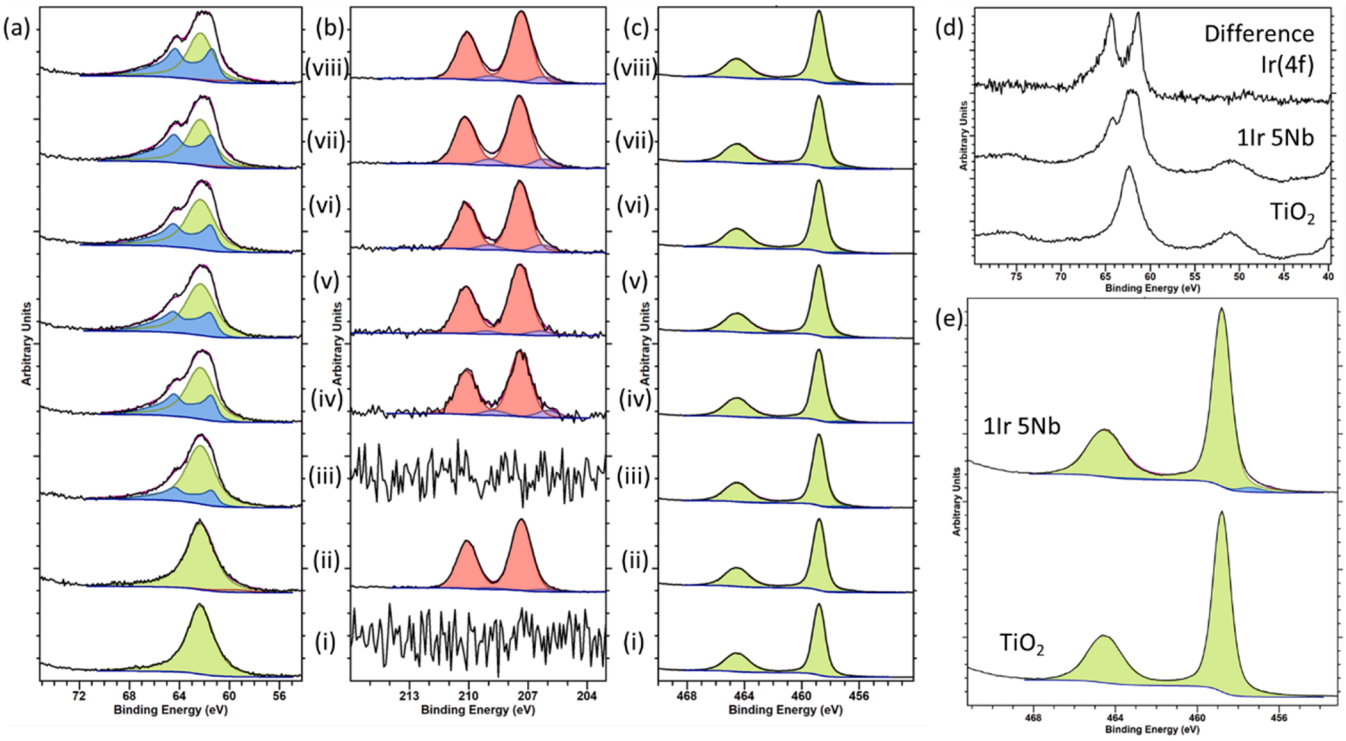

Fig. 9. (a) Ir(4 f)/Ti(3 s)/Nb(4 s), (b) Nb(3d), (c) Ti(2p) core-level spectra, where (i) TiO_2, (ii) Nb/TiO_2, (iii) Ir/TiO_2, (iv) 1Ir 0.5 Nb/TiO_2 (v) 1Ir 1 Nb/TiO_2, (vi) 1Ir 2 Nb/TiO_2, (vii) 1Ir 5 Nb/TiO_2 and (viii) 1Ir 10 Nb/TiO_2; (d) shows the difference of spectra used to confirm the Ir(4 f) peak shape, whilst (e) shows more clearly the presence of Ti^{3+} with respect to bare TiO_2.

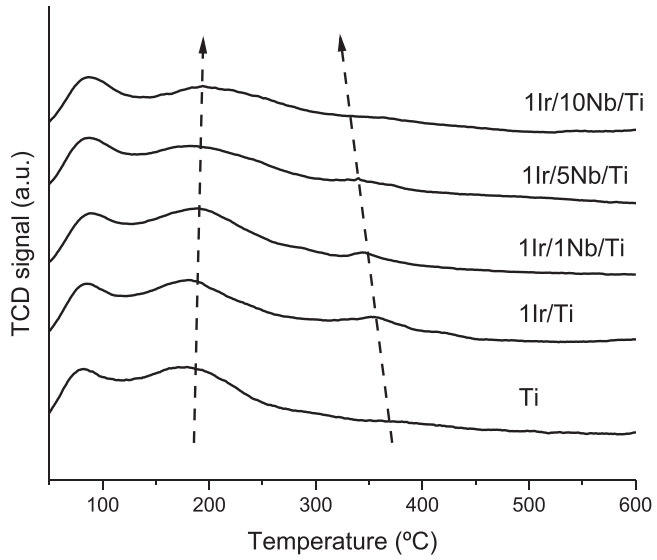

Fig. 10. Temperature programmed desorption of oxygen on Ir/Nb/Ti catalysts.

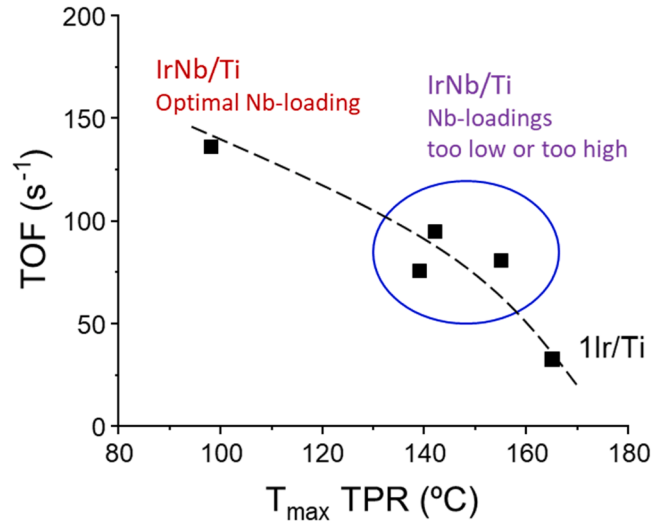

Fig. 11. Relationship between the temperature of the maximum of the most reducible TPR peak and the turnover frequency (x10^4) in propane oxidation. TOF is determined like in Table 2.

the temperature of the maximum decreases, likely suggesting a determining role of the reducibility on the catalytic activity.

This better reducibility must be related to the presence of surface Nb species, which play a catalytic role. Then, by XPS it has been observed that niobium, apart from the usual 5 + oxidation state presents a certain proportion with a 4 + oxidation state. This defective surface means the presence of surface oxygen vacancies, that can affect the oxygen mobility and therefore the reactivity. In fact, the most reactive catalyst (1Ir/5 Nb/Ti) is the one with the highest $Nb^{4+}/(Nb^{4+} + Nb^{5+})$ ratio. It must be mentioned that Nb^{4+} has been also detected in the Ir-free Nb/Ti catalyst but, in this case, there is no active site to activate the alkane, in contrast with the Ir-containing catalysts. Similarly, the presence of iridium and/or niobium has also meant the formation of defective Ti^{3+} species which is absent in the pure titania support. It is possible both Nb and iridium modify the environment of surface titania, which can modify the lability of oxygen species, being this effect more relevant for the optimum catalyst with 5 wt% Nb loading.

A closer look at the characterization results allows us to propose the reason for the promotional effect of Nb. Nb-free sample presents (apart from isolated IrOx species) nanoclusters of IrO_2, which are absent in the optimal Nb-containing IrTi catalyst, which only shows highly dispersed IrOx species into the TiO_2 structure. Then, it seems that the Nb promotes Ir incorporation into the TiO_2 network. This interesting surface configuration leads to weaker Ir-O bonds than those observed for the non-promoted catalyst, creating active sites more reducible and therefore more reactive.

Additionally, doping moderate amounts of Nb to titania decreases the number of strong acid sites and a weakening both strong and weak acid sites. However, high amounts of niobium exceeding the theoretical monolayer lead to an increased acidity as a result of the formation of Nb_2O_5 clusters. In the case of supported noble metal catalysts, the type of support strongly affects the electronic structure (the electron density of the active metal atoms). Thus, we have observed that the supports with high acidity (bare titania or titania with an excess of niobium) tend to draw electrons from the active iridium sites increasing the iridium-support interaction and decreasing the reducibility of IrOx sites and consequently the reactivity in the total oxidation reaction. Accordingly, the highest activity is achieved with the catalyst with the lowest and weakest acidity. Therefore, it seems that a combination of both effects, dispersion of IrOx active sites and weaker acidity, promote the catalytic activity of Nb doped samples.

In the case of Pd/TiO_2 catalysts, the addition of niobium also led to an improvement in the catalytic activity in the alkane total oxidation [17,44]. In these articles, it was observed that the presence of niobium increased oxygen mobility and produced new and highly reducible species. Similarly in V-promoted Pd/TiO_2 catalysts, the presence of a higher concentration of V^{4+} species apart from the majority V^{5+} species suggested an easier redox cycle and then increased the reactivity [45]. Then, it seems that in Pd/TiO_2 catalysts the main effect of adding low active promoters is the enhancement of the reducibility minimizing the Pd/support interaction. Therefore, the mechanism for the promotion by adding Nb to Ir/TiO_2 seems to be similar.

The influence of the presence of water and/or CO_2 in the feed was also studied (Fig. 12A) over the most active catalyst (1Ir/5 Nb/Ti). Meanwhile the addition of 2 vol% CO_2 did not mean any substantial difference compared to the standard experiment, the addition of 8 vol% steam led to a notable decrease in the propane conversion. As a positive feature, we want to mention that feeding steam no appreciable further decrease was observed with the time on line. It must be noted that after several experiments with or without water or carbon dioxide, the catalytic activity was fully restored, confirming the high robustness of this catalyst. The tolerance to water in the feed of this Nb-promoted Ir catalyst was compared with the Nb-free Ir-catalyst. This test was undertaken using propane and at a reaction temperature at which the propane conversion was ca. 75% (350ºC for the Nb-containing catalyst and 400ºC for the Nb-free catalyst). The presence of water has meant in both cases a decrease in the alkane conversion. However, the decrease in catalytic activity for the Nb-containing catalyst (ca. 30% drop) was less drastic than in the case of the Nb-free catalyst (ca. 55% drop). This different trend could be explained by a weaker acidity of the iridium active sites after niobium addition, as observed by NH_3-TPD, decreasing water competitive adsorption.

5. Conclusions

The addition of niobium to Ir/TiO_2 catalysts highly increases the catalytic activity for the total oxidation of a set of alkanes and their mixtures. Interestingly, these catalysts are highly stable and maintain the same level of conversion for at least 25–30 h. A part of this enhanced reactivity can be due to a higher amount of exposed active iridium species. However, the turnover frequency (per exposed active site) is markedly higher in bimetallic Ir/Nb-catalysts than in monometallic Ir/Ti catalysts, so other factors should be taken into account. Then, it seems that the promotional effect of niobium is mainly related to enhanced reducibility of the IrOx species, favoured by the lower acidity of the TiO_2

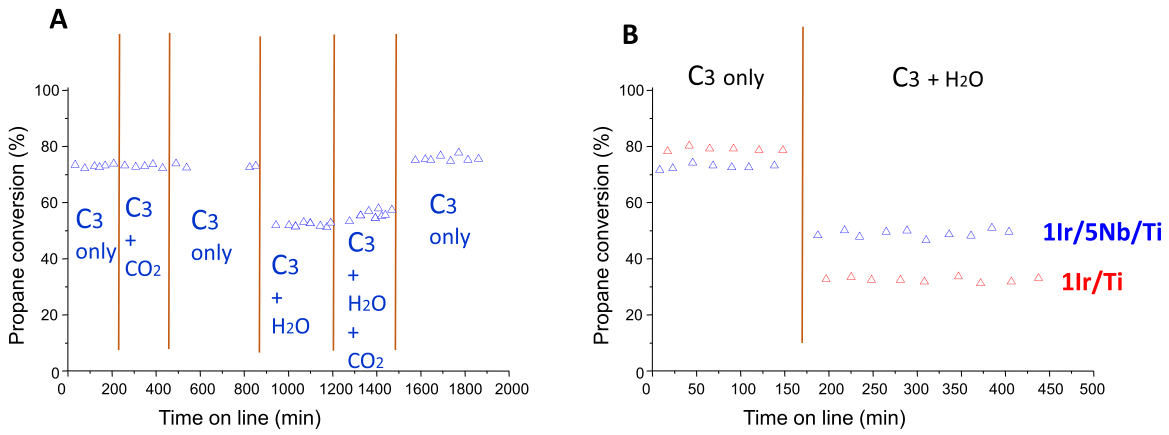

Fig. 12. A) Evolution of propane conversion in the presence of CO_2 and/or H_2O in the feed for 1Ir/5 Nb/Ti catalyst (Δ). Reaction condition in text and reaction temperature of 350ºC. B) Influence of the presence of steam in the feed for 1Ir/Ti catalyst (Δ) and 1Ir/5 Nb/Ti catalyst (Δ). Reaction condition in text and reaction temperature of 350ºC in the case of 1Ir/5 Nb/Ti catalyst and 400ºC in the case of 1Ir/Ti catalyst.

support observed after Nb incorporation. Then, if suitable amounts of Nb are present, isolated IrOx surface species seem to be the only surface species formed. However, the absence of niobium or the use of Nb-loadings higher than the theoretical monolayer leads to the formation of IrO_2 nanoclusters, which apparently are less reactive. A positive influence on the reactivity of both non-stoichiometric surface Nb^{4+} and Ti^{3+} species that generate oxygen vacancies influencing the reactivity is highly likely. This is the first case reported in which a promotional effect of doping by an inactive metal (such as Nb) is observed in supported Ir-catalyst for the total alkane oxidation, as it has been often observed in the scientific literature in Pd- or Pt-supported catalysts.

CRediT authorship contribution statement

Marvin Chávez: Investigation, Writing – original draft. **Adrián García:** Investigation, Data curation and Writing – original draft. **Rut Sanchis:** Methodology, Formal analysis **Clarisse Furgeaud:** Methodology, Formal analysis and Writing – original draft. **Alvaro Mayoral:** Formal analysis, Writing – review & editing **Raul Arenal:** Validation, Writing – review & editing **David J. Morgan:** Methodology, Formal analysis, Writing – original draft. **Stuart H. Taylor:** Conceptualization, Editing **Jose Manuel López:** Writing – review & editing **Tomás García:** Funding acquisition, Supervision, Conceptualization, Writing – review & editing **Benjamín Solsona:** Funding acquisition, Supervision, Conceptualization, Writing – review & editing.

Declaration of Competing Interest

The authors declare that they have no known competing financial interests or personal relationships that could have appeared to influence the work reported in this paper.

Acknowledgements

The authors would like to thank the Regional Government of Aragon (DGA) for the support provided under the research groups support programme (T04_20R). M. C-S would like to thank the University of Valencia and the vice-rector of international relations and cooperation for the fellowship through the young researcher's program (2019).

Appendix A. Supporting information

Supplementary data associated with this article can be found in the online version at doi:10.1016/j.jece.2022.108261.

References

[1] C. He, J. Cheng, X. Zhang, M. Douthwaite, S. Pattisson, Z. Hao, Chem. Rev. 119 (7) (2019) 4471–4568.
[2] B. Liu, J. Ji, B. Zhang, W. Huang, Y. Gan, D.Y.C. Leung, H. Huang, J. Hazard. Mater. 422 (2022), 126847.
[3] T. Yin, X. Meng, S. Wang, X. Yao, N. Liu, L. Shi, Sep. Purif. Technol. 280 (2022), 119634.
[4] M.S. Kamal, S.A. Razzak, M.M. Hossain, Atmos. Environ. 140 (2016) 117–134.
[5] X. Li, L. Zhang, Z. Yang, P. Wang, Y. Yan, J. Ran, Sep. Purif. Technol. 235 (2020), 116213.
[6] Y. Guo, M. Wen, G. Li, T. An, Appl. Catal. B Environ. 281 (2021), 119447.
[7] Z. Zhang, Z. Jiang, W. Shangguan, Catal. Today 264 (2016) 270–278.
[8] R.M. Harrison, J. Allan, D. Carruthers, M.R. Heal, A.C. Lewis, B. Marner, T. Murrells, A. Williams, Atmos. Environ. 262 (2021), 118592.
[9] H. Huang, Y. Xu, Q. Feng, D.Y.C.C. Leung, Catal. Sci. Technol. 5 (5) (2015) 2649–2669.
[10] S. Song, S. Zhang, X. Zhang, P. Verma, M. Wen Front. Mater. 7(October) (2020) 1–14.
[11] R. Spinicci, A. Tofanari, Appl. Catal. A Gen. 227 (1) (2002) 159–169.
[12] H.L. Tidahy, S. Siffert, J.-F.F. Lamonier, E.A. Zhilinskaya, A. Aboukaïs, Z.-Y. Y. Yuan, A. Vantomme, B.-L.L. Su, X. Canet, G. De Weireld, M. Frère, T.B. N'Guyen, J.-M.M. Giraudon, G. Leclercq, T.B. N'Guyen, J.-M.M. Giraudon, G. Leclercq, Appl. Catal. A Gen. 310 (2006) 61–69.
[13] J.-M.M. Giraudon, T.B. Nguyen, G. Leclercq, S. Siffert, J.-F.F. Lamonier, A. Aboukaïs, A. Vantomme, B.-L.L. Su, Catal. Today 137 (2) (2008) 379–384.
[14] V.P. Santos, S.A.C.C. Carabineiro, P.B. Tavares, M.F.R.R. Pereira, J.J.M.M. Órfão, J. L. Figueiredo, Appl. Catal. B Environ. 99 (1) (2010) 198–205.
[15] L. Schick, R. Sanchis, V. González-Alfaro, S. Agouram, J.M. López, L. Torrente-Murciano, T. García, B. Solsona, Chem. Eng. J. 366 (2019) 100–111.
[16] L. Schick, V. González-Alfaro, A. García, J.M. López, D.J. Morgan, S. Agouram, S. H. Taylor, T. García, B. Solsona, Chem. Eng. J. 417 (2021), 127999.
[17] M. Taylor, E.N. Ndifor, T. Garcia, B. Solsona, A.F. Carley, S.H. Taylor, Appl. Catal. A Gen. 350 (1) (2008) 63–70.
[18] L.S. Escandón, S. Ordóñez, F.V. Díez, H. Sastre, Catal. Today 78 (1) (2003) 191–196.
[19] T.V. Choudhary, S. Banerjee, V.R. Choudhary, Appl. Catal. A Gen. 234 (1–2) (2002) 1–23.
[20] J. Yan, L. Wang, Y. Guo, Y. Guo, Q. Dai, W. Zhan, Appl. Catal. A Gen. 628 (2021), 118398.
[21] Z. Chen, J. Li, P. Yang, Z. Cheng, J. Li, S. Zuo, Chem. Eng. J. 356 (2019) 255–261.
[22] Y. Jing, G. Wang, K.W. Ting, Z. Maeno, K. Oshima, S. Satokawa, S. Nagaoka, K. Shimizu, T. Toyao, J. Catal. 400 (2021) 387–396.
[23] H. Ohtsuka, Catal. Lett. 141 (3) (2011) 413–419.
[24] A. Aguilar-Tapia, R. Zanella, C. Calers, C. Louis, L. Delannoy, Phys. Chem. Chem. Phys. 17 (42) (2015) 28022–28032.
[25] L. Torrente-Murciano, B. Solsona, S. Agouram, R. Sanchis, J.M. López, T. García, R. Zanella, Catal. Sci. Technol. 7 (13) (2017) 2886–2896.
[26] E. Heracleous, A.A. Lemonidou, J. Catal. 270 (1) (2010) 67–75.
[27] M.O. Guerrero-Pérez, M.A. Bañares, Catal. Today 142 (3) (2009) 245–251.
[28] M.O. Guerrero-Pérez, Catal. Today 354 (2020) 19–25.
[29] J.C. Rooke, T. Barakat, M.F. Finol, P. Billemont, G. De Weireld, Y. Li, R. Cousin, J.-M. Giraudon, S. Siffert, J.-F. Lamonier, B.L. Su, Appl. Catal. B Environ. 142–143 (2013) 149–160.
[30] Q. Wu, J. Zhao, G. Qin, C. Wang, X. Tong, S. Xue, Appl. Catal. B Environ. 142–143 (2013) 142–148.
[31] P. Papaefthimiou, T. Ioannides, X.E. Verykios, Appl. Catal. B Environ. 15 (1) (1998) 75–92.

[32] T. Garcia, B. Solsona, D. Cazorla-Amorós, Á. Linares-Solano, S.H. Taylor, Appl. Catal. B Environ. 62 (1) (2006) 66–76.
[33] N. Fairley, V. Fernandez, M. Richard-Plouet, C. Guillot-Deudon, J. Walton, E. Smith, D. Flahaut, M. Greiner, M. Biesinger, S. Tougaard, D. Morgan, J. Baltrusaitis, Appl. Surf. Sci. Adv. 5 (2021), 100112.
[34] S. Tanuma, C.J. Powell, D.R. Penn, Surf. Interface Anal. 35 (3) (2003) 268–275.
[35] M.N. Taylor, W. Zhou, T. Garcia, B. Solsona, A.F. Carley, C.J. Kiely, S.H. Taylor, J. Catal. 285 (1) (2012) 103–114.
[36] J.M. Jehng, I.E. Wachs, Chem. Mater. 3 (1) (1991) 100–107.
[37] G.B. McVicker, R.T.K. Baker, R.L. Garten, E.L. Kugler, J. Catal. 65 (1) (1980) 207–220.
[38] B.J. Kip, F.B.M. Duivenvoorden, D.C. Koningsberger, R. Prins, J. Catal. 105 (1) (1987) 26–38.
[39] C. Zhao, I.E. Wachs, Catal. Today 118 (3) (2006) 332–343.
[40] Y. Cheng, I.E. Wachs, J. Catal. 217 (2) (2003) 468–477.
[41] F.L. Deepak, A. Mayoral, A. Raul Advanced Transmission Electron Microscopy, first ed., Springer International Publishing, 2015.
[42] S.J. Freakley, J. Ruiz-Esquius, D.J. Morgan, Surf. Interface Anal. 49 (8) (2017) 794–799.
[43] Y. Jian, Z. Jiang, C. He, M. Tian, W. Song, G. Gao, S. Chai, Catal. Sci. Technol. 11 (3) (2021) 1089–1097.
[44] M.F. Finol, J. Rooke, B.-L. Su, M. Trentesaux, J.-M. Giraudon, J.-F. Lamonier, Catal. Today 192 (1) (2012) 154–159.
[45] T. Garcia, B. Solsona, S.H. Taylor, Catal. Lett. 97 (1) (2004) 99–103.